

Two-dimensional vortex behavior in highly underdoped $\text{YBa}_2\text{Cu}_3\text{O}_{6+x}$ observed by scanning Hall probe microscopy

J. W. Guikema,^{1,*} Hendrik Bluhm,¹ D. A. Bonn,² Ruixing Liang,² W. N. Hardy,² and K. A. Moler^{1,†}

¹*Departments of Physics and of Applied Physics, Stanford University, Stanford, CA 94305*

²*Department of Physics and Astronomy, University of British Columbia, Vancouver, BC, Canada V6T 1Z1*

(Dated: February 10, 2008)

We report scanning Hall probe microscopy of highly underdoped superconducting $\text{YBa}_2\text{Cu}_3\text{O}_{6+x}$ with T_c ranging from 5 to 15 K which showed distinct flux bundles with less than one superconducting flux quantum (Φ_0) through the sample surface. The sub- Φ_0 features occurred more frequently for lower T_c , were more mobile than conventional vortices, and occurred more readily when the sample was cooled with an in-plane field component. We show that these features are consistent with kinked stacks of pancake vortices.

PACS numbers: 74.25.Ha, 74.25.Qt, 74.72.Bk

I. INTRODUCTION

Cuprate superconductivity occurs mainly in the ab direction on the CuO_2 planes. This quasi-two-dimensional nature manifests itself in the anisotropy between the c -axis penetration depth (λ_c) and the in-plane penetration depth (λ_{ab}). Clem¹ showed that in highly anisotropic layered superconductors a c -axis vortex can be viewed as a stack of magnetically coupled “pancake” vortices, one in each layer. This formulation suggested the possibility for novel vortex behavior and has become a major part of the phenomenological understanding of cuprate superconductors. However, direct observations of separated pancakes or pancake stacks have been rare.^{2,3}

In this paper, we present scanned probe microscopy of magnetic flux in highly underdoped $\text{YBa}_2\text{Cu}_3\text{O}_{6+x}$ (YBCO) single crystals. We observed nearly isolated flux features with less than one flux quantum ($\Phi_0 = hc/2e = 20.7 \text{ G}\mu\text{m}^2$) through the sample surface, which we call “partial vortices”. A model of separated pancake vortex stacks, similar to a kinked structure suggested by Benkraouda and Clem,⁴ but with a more important role for pinning, agrees well with our observations.

Non-quantized flux in superconductors has been observed experimentally, arising for different reasons. Geim et al.⁵ observed non-quantized flux penetration in mesoscopic thin film samples of aluminum due to two effects: the proximity of the vortices to the sample edge, and a surface barrier to flux penetration. Sub- Φ_0 flux has been imaged in YBCO thin films along grain boundaries separating regions of the crystal rotated 45° about the c -axis due to the d -wave symmetry of the pairing state in combination with facets along the grain boundary.^{6,7} For our measurements discussed here, the vortices were far from the edge and there were no rotations of the crystal axes aside from 90° twinning, so neither of these mechanisms applies. Our observations of seemingly isolated fractional fluxes in a bulk material far from any boundaries requires a different explanation.

This paper is organized as follows. Section II describes the growth and preparation of the high-quality highly

underdoped YBCO crystals and introduces the scanning Hall probe microscope. Section III discusses Hall probe observations of partial vortices, and in Sec. IV we model these partial vortices as kinked stacks of two-dimensional (2D) pancake vortices. Section V presents other experimentally observed properties, which are all consistent with the kinked vortex picture. Finally, in Sec. VI we discuss the partial vortices in light of energy costs and pinning. The Appendix of this paper discusses the in-plane penetration depth extracted from fits to vortices in the YBCO.

II. SAMPLES AND METHODS

The $\text{YBa}_2\text{Cu}_3\text{O}_{6+x}$ crystals, with x from 0.34 to 0.375, are grown with a self-flux method in BaZrO_3 crucibles detailed elsewhere.^{8,9} After growth, the desired oxygen content is set during a $900\text{--}930^\circ\text{C}$ anneal in flowing oxygen, then oxygen inhomogeneities are removed during a $1\text{--}2$ week 570°C anneal in a small tube with YBCO ceramic at the same oxygen content. Initially, after quenching to 0°C , the crystals are non-superconducting, but annealing at room temperature allows the oxygen atoms to order into Ortho-II (every other chain empty) chain fragments whose increasing length provides the carrier doping in the CuO_2 planes.⁹ The superconducting transition temperature (T_c) increases with room temperature annealing until saturation is reached after several weeks, giving final T_c values of $5\text{--}20$ K with bulk susceptibility transition widths (10%–90%) of less than 2 K.⁹ This early generation of underdoped samples sometimes had a small ($<2\%$) volume fraction of the $50\text{--}60$ K T_c phase of Ortho-II YBCO, as observed in magnetization measurements.¹⁰ During the room temperature annealing, a single crystal can be observed at a range of T_c values. The platelet shaped crystals are about $1 \text{ mm} \times 1 \text{ mm}$ wide, with their surface parallel to the ab -plane, and are typically $10\text{--}100 \mu\text{m}$ thick. As grown, the crystals have twinning boundaries, but they can be detwinned under uniaxial pressure at elevated temperatures.

Our most detailed observations of sub- Φ_0 partial vortices were made with a scanning Hall probe microscope,^{11,12,13,14} described in Ref. 11. Scanning Hall probe microscopy of single vortices is an established technique^{12,13,14} first demonstrated by A. M. Chang et al.¹² Our Hall probe was made from GaAs/AlGaAs two-dimensional electron gas and had lithographic size $0.5\text{ }\mu\text{m} \times 0.5\text{ }\mu\text{m}$. The Hall probe measures the perpendicular magnetic field in the active area (with a constant offset). The Hall cross was covered by a thin film of gold which was grounded during operation. This gate prevented any stray electric charges on the sample surface from perturbing the Hall signal. For positioning in the z direction, the probe is mounted on the end of a thin aluminum diving board which forms a parallel plate capacitor with a copper pad underneath it. As the tip of the probe approaches the sample, we monitor the capacitance and can ideally determine the location of the sample surface to within 10 nm. This touchdown procedure is repeated at multiple locations within the scan area and then the probe is scanned in a plane just above the sample surface. The minimum height of the Hall cross active area above the sample surface is determined by the sample-probe alignment and for these measurements was $0.4\text{ }\mu\text{m}$ or larger due to geometric constraints. The lateral scan range of the microscope at 4 K is $60\text{ }\mu\text{m}$ and the sample can also be repositioned using xy stick-slip course motion. For improved signal-to-noise ratio, we averaged multiple images (having checked that the consecutive images did not show changes). We sometimes used an $8\text{ }\mu\text{m} \times 8\text{ }\mu\text{m}$ scanning superconducting quantum interference device (SQUID) with better flux sensitivity, but worse spatial resolution than the Hall probe. The cryostat was inside triple-layer mu-metal magnetic shielding with a residual field of less than 25 mG.

The main results presented in this paper are from an $8\text{ }\mu\text{m}$ thick twinned $\text{YBa}_2\text{Cu}_3\text{O}_{6.375}$ crystal imaged at eight stages during the room temperature oxygen ordering annealing. The annealing took place in the microscope in a helium atmosphere. After 36 hours of annealing, the crystal had $T_c \sim 5.1\text{ K}$ and transition width $\Delta T_c \sim 3\text{ K}$. Further annealing gave a range of T_c values all having $\Delta T_c < 1.5\text{ K}$. The maximum measured T_c was 14.7 K (Fig. 1 inset). T_c values were obtained in situ in an 8.3 mHz applied field of amplitude 0.20–0.25 Oe (Fig. 1). The transitions are described as midpoint T_c 's with full widths limited by the $\sim 10\%$ resolution of the susceptibility measurement.

We also imaged flux in nine other similarly prepared $\text{YBa}_2\text{Cu}_3\text{O}_{6+x}$ crystals with x in the range 0.35–0.375 and T_c 's in the range 7–17 K. Each of these crystals was studied at only one T_c value. Sub- Φ_0 flux features were seen in the three crystals with the lowest $T_c \sim 7\text{ K}$ values.¹¹ The higher T_c samples with $T_c \gtrsim 11\text{ K}$ only showed flux consistent with conventional Φ_0 vortices. We also imaged vortices in Ortho-II ($T_c \approx 60\text{ K}$) and near-optimally doped YBCO crystals and did not see any evidence of sub- Φ_0 partial vortices.

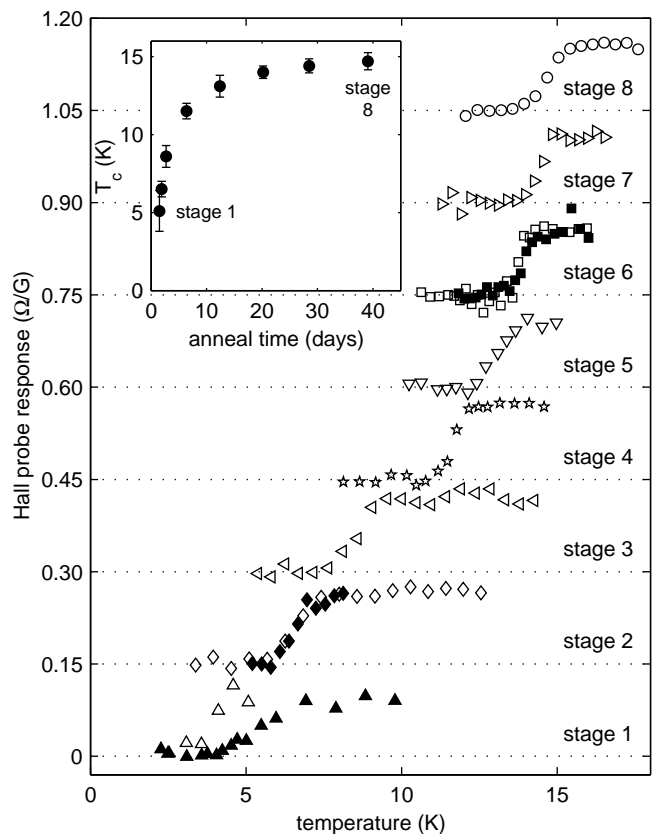


FIG. 1: Superconducting transitions in the $\text{YBa}_2\text{Cu}_3\text{O}_{6.375}$ crystal measured by in situ magnetic susceptibility with the Hall probe in an applied 8.3 mHz field of amplitude 0.25 Oe for stages 1–2 and 0.20 Oe for stages 3–8. Stages offset by $0.15\text{ }\Omega/\text{G}$. Filled symbols are second measurements at different locations. A Hall probe response of $R_H = 0.115 \pm 0.015\text{ }\Omega/\text{G}$ indicates no measurable Meissner response, while $0\text{ }\Omega/\text{G}$ indicates full shielding. Inset: Midpoint transition temperature (T_c) versus cumulative room temperature annealing time for the $\text{YBa}_2\text{Cu}_3\text{O}_{6.375}$ crystal. Vertical bars indicate the full transition width, limited by our measurement resolution.

III. FLUX IMAGES

We saw over 100 sub- Φ_0 flux features in the $\text{YBa}_2\text{Cu}_3\text{O}_{6.375}$ crystal while tuning T_c from 5 to 15 K. We also observed more than 300 apparently full Φ_0 vortices, which were dominant for $T_c > 11.5\text{ K}$. Typical Hall probe images are shown in Fig. 2 for a range of T_c . These images were taken at low temperatures ($T < T_c/2$) after field-cooling the crystal at about 3 K/min in a perpendicular field. Though not necessary, the images were taken after turning off the applied field at low temperature. Images taken before and after turning off the field looked identical. No flux features were observed when we cooled the sample in zero field. The images were not all taken at the same place on the crystal, because we occasionally used our course motion capability to move the sample in order to view nearby regions.

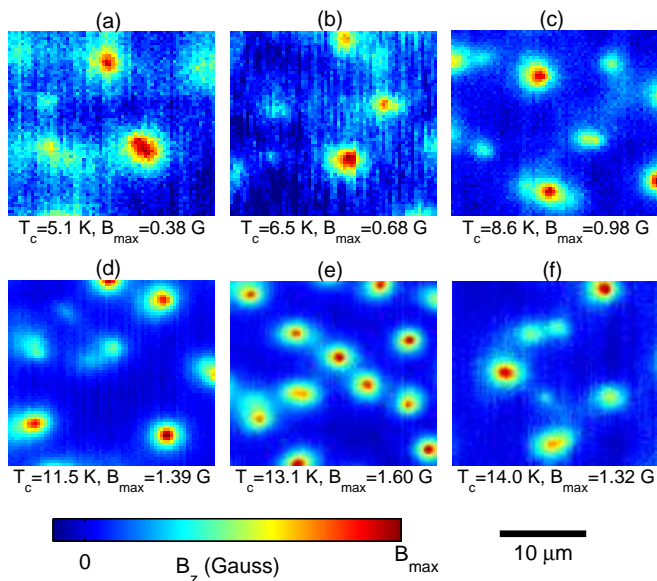


FIG. 2: (Color). Hall probe images of magnetic flux in the $\text{YBa}_2\text{Cu}_3\text{O}_{6.375}$ crystal for increasing T_c (stages 1–6). The probe’s size was nominally $0.5 \mu\text{m}$. The circular features with largest B_z are likely straight pancake vortex stacks (“full vortices”), while the dimmer and sometimes non-circular features are identified as segments of kinked pancake vortex stacks (“partial vortices”). The applied field H_z while cooling through T_c and the temperature T at which each image was acquired were (a) 0.15 Oe and 2.0 K, (b) 0.21 Oe and 2.3 K, (c) 0.21 Oe and 2.4 K, (d) 0.21 Oe and 2.2 K, (e) 0.43 Oe and 4.3 K, and (f) 0.20 Oe and 4.1 K. A constant background has been subtracted from each image. For (f), low frequency telegraph noise in the Hall probe signal was subtracted from the raw images before averaging.

The images in Fig. 2 show flux features that can be divided into two types. We identify the brightest features, which are close to circular, as conventional or “full” vortices. They carry total flux Φ_0 through the crystal surface, within experimental error. The full vortices increased in peak B_z and decreased in width as T_c increased, likely due to changes in the in-plane penetration depth (see Appendix). Other features have a smaller peak B_z and appear either circular, elongated, or with tails. We call these features “partial vortices” because they carry less than Φ_0 of total flux through the surface. When the sample was cooled in a perpendicular field, partial vortices accounted for more than half of the observed flux features for $T_c \leq 11.5$ K (stages 1–4), but dropped to less than 10% for $T_c > 14$ K (stages 7 and 8).¹¹ We will show that the partial vortices can be explained by non-axial arrangements of 2D pancake vortices.

The flux carried by the partial vortices was not restricted to discrete fractions of Φ_0 , as shown by a tally of the ratios of the peak B_z of a partial vortex to the peak B_z of a full vortex in the same image (Fig. 3). The peak B_z ratio for a partial vortex does not translate directly to the fraction of a Φ_0 through the surface, but nonethe-

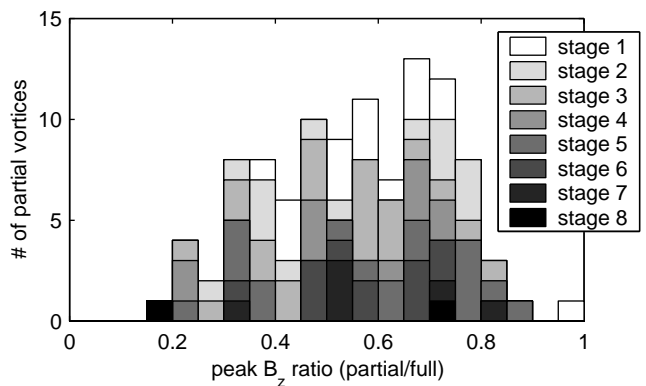


FIG. 3: Histogram of partial vortex peak field as a fraction of full vortex peak field in the $\text{YBa}_2\text{Cu}_3\text{O}_{6.375}$ crystal. Sample was cooled to low temperature in a perpendicular field before each image was acquired. Total bar heights show data from all anneal stages (all T_c values).

less, Fig. 3 indicates that the partial vortices occurred for a range of magnitudes. It is not feasible to directly tally the flux of each partial vortex without large errors because the field from nearby vortices in many cases interferes with the integration.

A tempting hypothesis is that a partial vortex consists of a straight stack of pancake vortices, one in each layer, with some unusual mechanism by which the total flux is permitted to be less than Φ_0 . In this case, the field profile of a partial vortex above the sample surface could be calculated using the anisotropic London model (see Eq. (A.1) in the Appendix) except with a flux smaller than Φ_0 . If the in-plane penetration depth was assumed to be constant throughout the sample at each T_c , then the peak B_z ratio given in Fig. 3 would be equivalent to the fraction of a flux quantum carried by the partial vortex. However, we do not believe this hypothesis is the best explanation of our data.

The main sources of error in the peak B_z ratios were noise in the data and error in background determination, roughly 50 mG each. This gives an error in the peak B_z ratios of $\sim 5\%$ at the higher T_c values, and several times this for the lowest T_c . Counts may also be missing at the ends of the histogram, since a partial vortex with close to full peak would likely be mistaken as a full vortex and those with very small peak field may have been lost in the noise. We omitted some flux features from the histogram if they could not be clearly identified as partial or full vortices. We also omitted whole images if they had high noise or did not contain a full vortex, the latter being particularly an issue for the lowest anneal stage where full vortices were rare. Only 21% of the images from stage 1 were included in the tally, while most images from subsequent stages were included.

IV. KINKED PANCAKE STACKS

In this section we discuss a model in which the partial vortices result from kinked stacks of pancake vortices. We show that the model quantitatively describes the most circular partial vortices, and qualitatively describes the shapes and tails of the non-circular ones.

In Ref. 1, Clem introduced the idea of 2D pancake vortices as the basic building blocks of 3D vortices in highly anisotropic superconductors consisting of weakly Josephson coupled layers. Even when the interlayer Josephson coupling is not negligible, the vortex structure can be described as a superposition of 2D pancake vortices and short sections of Josephson vortices (called “strings”) connecting pancakes in adjacent layers.¹⁵ Clem¹ also showed that for a vortex aligned along the c -axis, a straight stack of 2D pancake vortices gives the same result as an ordinary 3D vortex in the anisotropic London model. However, Benkraouda and Clem⁴ proposed that a tilted pancake stack may lower its energy by instead forming a kinked structure similar to the one shown in Fig. 4(c), rather than maintaining a homogeneous tilt angle. Our observations of partial vortices suggest such configurations of kinks and short pancake stacks, which are stabilized by pinning effects.

Compared to optimally doped YBCO, where $\gamma = \lambda_c/\lambda_{ab} \approx 5.5 \pm 1$,¹⁶ our highly underdoped $\text{YBa}_2\text{Cu}_3\text{O}_{6+x}$ ($x \approx 0.35\text{--}0.375$) crystals are much more anisotropic. Microwave measurements in similar samples found zero temperature values $\lambda_c(0) \approx 100 \mu\text{m}$ for $T_c \approx 6 \text{ K}$, and $\lambda_c(0) \approx 40 \mu\text{m}$ for $T_c \approx 15 \text{ K}$.¹⁷ The zero temperature in-plane penetration depth can be obtained from recent measurements¹⁸ of $H_{c1}(0)$ in similar crystals which found that the power law $H_{c1}(0) = 0.366 T_c^{1.64}$ (Oe) fit H_{c1} vs. T_c data well for $T_c \leq 22 \text{ K}$. Using $H_{c1} = \Phi_0(\ln(\kappa) + 0.5)/(4\pi\lambda_{ab}^2)$ and $\kappa \approx 40$ (Ref. 19) gives $\lambda_{ab}(0) = 1.00 \mu\text{m}$ and $0.47 \mu\text{m}$ for $T_c = 6 \text{ K}$ and 15 K , respectively. These λ_{ab} values are in agreement with values we obtained from fits to Hall probe vortex images from our variable T_c $\text{YBa}_2\text{Cu}_3\text{O}_{6.375}$ crystal as discussed in the Appendix. Thus $\gamma \approx 100$ for $T_c \approx 6 \text{ K}$ and $\gamma \approx 85$ for $T_c \approx 15 \text{ K}$ in these crystals.

Since the 2D single layer screening length $\Lambda = 2\lambda_{ab}^2/s \approx 1 \text{ mm}$ is greater than λ_c in our highly underdoped YBCO crystals (the bilayer spacing in YBCO is $s = 1.17 \text{ nm}$), interlayer Josephson coupling is not negligible¹ and the notion of purely magnetically coupled pancakes is not entirely accurate. However, due to the large values of λ_c and γ , the additional attraction between separated pancake stacks due to Josephson strings is smaller than the magnetic interaction, as will be discussed in Sec. VI. Thus the pancake vortex plus Josephson string picture should be at least qualitatively appropriate for these samples.

To show that short pancake stacks can explain our observations, we consider the magnetic field that a straight partial stack extending from z_i to z_f ($z_i < z_f \leq 0$) generates above the $z = 0$ surface of a layered superconductor

assumed to be much thicker than λ_{ab} . It was shown in Ref. 15 that the z component of the magnetic field at a height z above the surface and a radius r from the vortex axis is

$$B_z(r, z) = \frac{\Phi_0}{2\pi\lambda_{ab}^2} \int_0^\infty dq \frac{q e^{-qz} J_0(qr)}{Q(Q+q)} (e^{Qz_f} - e^{Qz_i}), \quad (1)$$

where $Q = \sqrt{q^2 + \lambda_{ab}^{-2}}$ and the layer spacing s is much smaller than both z and λ_{ab} . If the partial stack extends from $|z_i| \gg \lambda_{ab}$ to $z_f = 0$, Eq. (1) gives the field of a conventional 3D vortex (Eq. (A.1)). Integrating Eq. (1) gives total flux

$$\Phi = \Phi_0 (e^{z_f/\lambda_{ab}} - e^{z_i/\lambda_{ab}}) \quad (2)$$

through the $z = 0$ surface of a superconducting half space for a partial vortex extending from z_i to z_f .^{15,20} If an otherwise straight vortex stack has one kink at a depth $z = -d$, the total flux through the surface from the lower and upper partial stacks is $\Phi_0 e^{-d/\lambda_{ab}}$ and $\Phi_0 (1 - e^{-d/\lambda_{ab}})$, respectively. The total flux is Φ_0 , as expected.

To compare the kinked stack model with our observations, we fit the two partial vortices labeled in Fig. 4(a) to a model of a pancake stack with one kink. Figure 4(b) shows that partial vortex #1 has a narrower profile, so we chose it as the upper stack. Adding the field profiles (Eq. (1)) of all the partial stacks in a kinked stack gives the field profile of a straight stack (full vortex). Figure 4(b) shows that the cross section through a full vortex is similar to the sum of the cross sections through partial vortices #1 and #2.

Using non-linear regression, we fit the portion of the image shown in Fig. 4(d) inside the oval to a numerical approximation of Eq. (1) with one expression each for the lower ($-\infty$ to $-d$) and upper ($-d$ to 0) partial pancake stacks. Free fit parameters were the depth of the split, d , and the radial centers (x_1, y_1) and (x_2, y_2) of each partial stack (Fig. 4(c)). Fixed input values were $z = 1.0 \mu\text{m}$ and $\lambda_{ab} = 0.65 \mu\text{m}$. This λ_{ab} was obtained from a 2D fit to the full vortex labeled ‘FV’ in Fig. 4(a) by the method described in the Appendix. Our fit gives a depth of the kink $d = 0.36 \mu\text{m}$ and lateral displacement at the kink (kink length) $\rho = \sqrt{(x_1 - x_2)^2 + (y_1 - y_2)^2} = 5.3 \mu\text{m}$. Figure 4(e) shows a 2D color plot of the fit and (f) shows cross-sections of the data and fit images along the dotted lines. Kinked or separated pancake vortex stacks is a plausible interpretation of our observations since, as Fig. 4 shows, the model fits well to our data.

This partial vortex pair was ideal for fitting because there appeared to be only a single kink within a few λ_{ab} of the surface and the partial stacks were well defined and circular. In most of our partial vortex images there were multiple kinks in a stack or several intermingled kinked stacks. In these cases, fitting the data would be more complicated. It was also common for partial vortices to have non-uniform shapes (see Fig. 2) which do

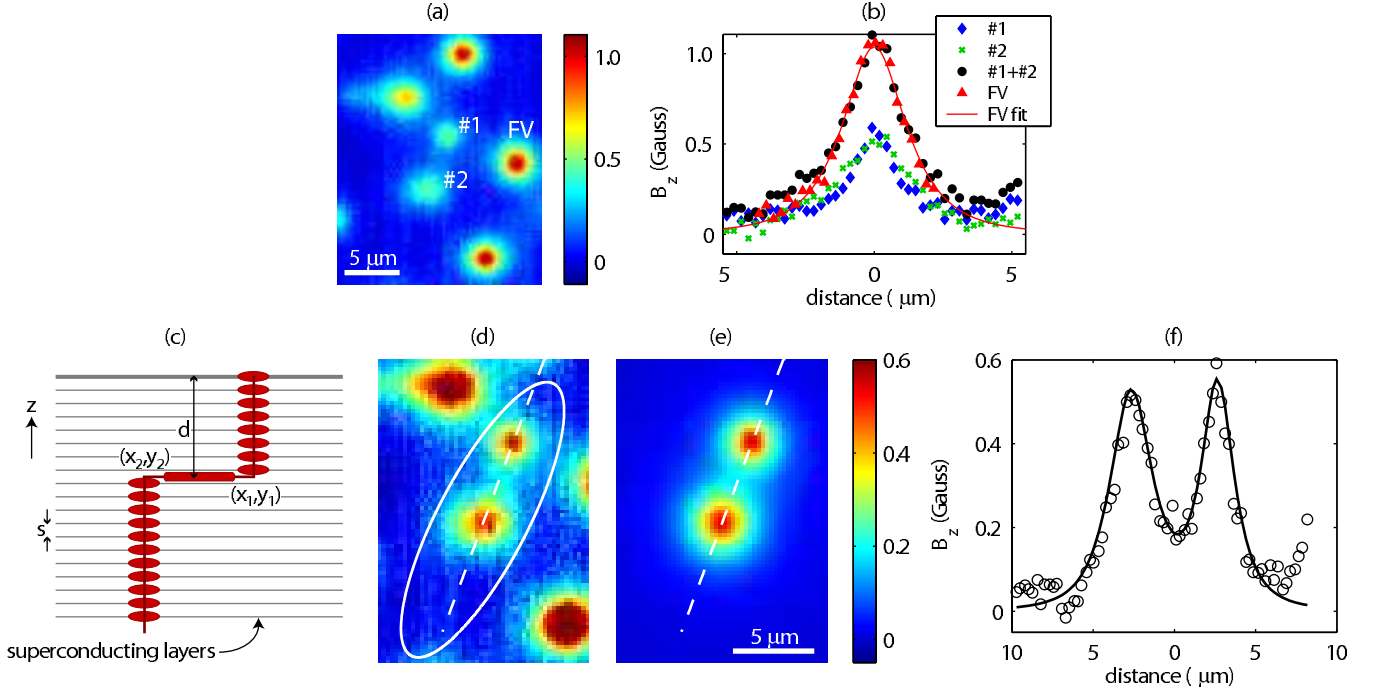


FIG. 4: (Color). Fit to a kinked pancake vortex stack in the $\text{YBa}_2\text{Cu}_3\text{O}_{6.375}$ at anneal stage 6 ($T_c = 14.0$ K) at $T = 4$ K. (a) Hall probe image containing partial vortices labeled #1 and #2. The 3 brightest features are full vortices. (b) Horizontal cross sections through the partial vortices, the sum of the partial vortices, and the full vortex labeled FV in (a). The solid line is from a 2D fit to the FV with $z = 1.0$ μm as a fixed parameter and $\lambda_{ab} = 0.65$ μm as a fit parameter. (c) Sketch of the assumed geometry of the kinked pancake stack, not to scale. (d) Zoom in of image (a) with the color scale adapted to the signal range of the partial vortices. (e) Fit to the partial vortices within the white oval in (d) as discussed in the text. $d = 0.36$ μm and kink length is 5.3 μm. (f) Cross-sections through the data (circles) and fit (line) along the dashed lines in (d) and (e).

not strictly agree with the model of one or a few kinks in a pancake stack. Elongated partial vortices and those with apparent tails, such as the partial vortex to the upper left of #1 in Fig. 4(a), could be the result of many closely spaced kinks, a tilt of a partial stack, or even a non-uniform staggering of pancakes from layer to layer. In each of these scenarios the displacement between adjacent pancakes would be smaller than the Hall probe spatial resolution. Though the kinked stack model cannot be used to fit irregularly shaped partial vortices without many free parameters, the underlying phenomenon is similar, with 2D pancake vortices playing a critical role.

V. OTHER CHARACTERISTICS

A number of observed properties of these partial vortices further substantiate the partial pancake stack interpretation as well as give further insight into their stability and pinning. Partial vortices occurred in groups, preferred certain regions in the crystal, were more mobile than full vortices, and were more likely to be formed by cooling in a tilted field.

The observed grouping of partial vortices is necessary for a kinked pancake stack, since all pancake vortices near the crystal surface carry flux through the surface which

collectively adds to Φ_0 . We observed partial vortices up to tens-of-microns away from others in a group, so even if a partial vortex appeared isolated, other segments may have been outside the image area. One caveat would be if there were subsurface vortex termination, which could occur for small sample size.²¹

Partial vortices showed a tendency to prefer certain regions of the crystal, even after a room temperature annealing. This was especially noticeable for the later anneal stages (higher T_c) for which partial vortices were rare. This may indicate that kinks occurred preferentially in regions of the sample which were different from the bulk, perhaps with higher disorder, more pinning sites, or weaker superconductivity. At the lowest T_c stage, we observed that partial vortices were more likely to pin where the tip of the Hall probe sat when the probe's active area was centered over the scan area. This was the location of the probe during cooldown through T_c and also the place where the z approach was most often performed to determine the location of the sample. The vortices may have been preferentially attracted to the location of the probe's tip, or the repeated contact with the sample in that location could have created pinning sites.

We also found that partial vortices were more mobile than apparent full vortices in the same samples. For

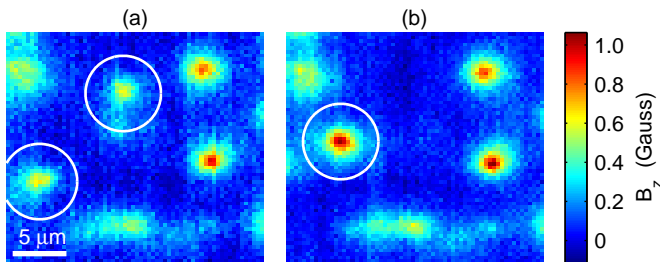


FIG. 5: (Color). Partial vortices coalesced during sample coarse motion ($T = 2.4$ K). (a) Hall probe image after cooling through $T_c = 8.6$ K in $H_z = 0.21$ Oe applied field. White circles identify two partial vortices. (b) After slight z coarse motion of the sample. Comparison of the images suggests that the partial vortices in (a) collapsed to one full vortex in (b).

example, partial vortices sometimes moved or coalesced after stick-slip coarse motion of the sample holder in the xy or z directions. This was not observed for full vortices. Figure 5 shows Hall probe images before and after several ramps of the voltage on the z piezoelectric and slight z coarse motion. Two partial vortices of similar peak amplitude in Fig. 5(a) appeared to coalesce into one full vortex in Fig. 5(b). Motion of partial vortices during coarse motion could be due to stray fields from the stick-slip high voltage pulses, which might create forces large enough to unpin some partial vortices. Once unpinned, a kinked stack could realign to a straight stack as favored by electromagnetic coupling of the pancakes and by any Josephson coupling.

To encourage partial vortex formation, we cooled the sample in a magnetic field with a horizontal component to reduce the energy cost of a kink. With the $\text{YBa}_2\text{Cu}_3\text{O}_{6.375}$ crystal almost fully annealed with $T_c = 14.4$ K (stage 7), the sample was cooled through T_c in an applied field $\vec{H} = H_x\hat{x} + H_z\hat{z}$. The vortex arrangement did not change when the field was turned off at 4 K. The images in Fig. 6 show increased numbers of partial vortices with increased H_x . The magnitude of H_z determined the density of flux observed in the images. The horizontal field may have caused pancakes within a stack to pin at large displacements with respect to each other as T was lowered through T_c . Since the flux arrangement did not change when the field was turned off, the pinning must have been sufficiently strong to overcome the restoring forces favoring a straight stack.

After cooling in a tilted field, we observed a change in the flux arrangement after the temperature was raised but still kept below T_c . As shown in Fig. 7(a), the $\text{YBa}_2\text{Cu}_3\text{O}_{6.375}$ sample with $T_c = 14.4$ K (stage 7) was cooled to 3 K in a field $\vec{H} = 2.0\hat{x} + 0.25\hat{z}$ Oe, where H_x was chosen to induce partial vortices. While at 3 K, the applied field was turned off and no change was observed. Then the sample was warmed to $T = 6.6$ K, cooled back to 3 K, and imaged again. This cycle was repeated several times with successively higher maximum T . After all cy-

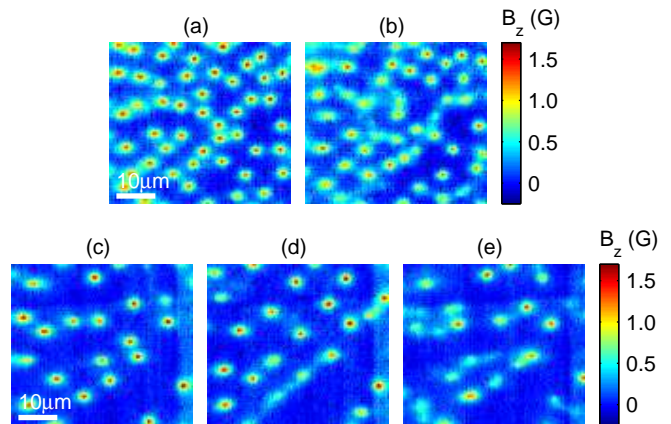


FIG. 6: (Color). Effect of an in-plane field on partial vortex formation in $\text{YBa}_2\text{Cu}_3\text{O}_{6.375}$. $T_c = 14.4$ K and $T = 4$ K for all the images. Field-cooled through T_c in $H_z = 0.50$ Oe and (a) $H_x = 0$, (b) $H_x = 2.3$ Oe. Field-cooled through T_c in $H_z = 0.20$ Oe and (c) $H_x = 0$, (d) $H_x = 1.2$ Oe, (e) $H_x = 2.3$ Oe. Images acquired in zero applied field. The x -direction is horizontal and z is out of the page.

cles, the flux arrangement changed. Vortices created by cooling through T_c in $\vec{H} = 0.25\hat{z}$ Oe did not show any motion after similar thermal cycling (Fig. 7(b)). These observations indicate high metastability of the vortices for cooling in non-zero H_x , as there are many possible structures consisting of pancake vortices and Josephson vortices in layered superconductors when cooled in a tilted field.

VI. DISCUSSION

The high-quality fit of the kinked stack model to our measured field profiles (Sec. IV), as well as the other observed properties of the sub- Φ_0 features (Sec. V), suggest that we have observed kinked pancake vortex stacks in the highly underdoped $\text{YBa}_2\text{Cu}_3\text{O}_{6+x}$ crystals. The large anisotropy and large λ_c in these crystals suggest that it is reasonable to think of vortices as being composed of 2D pancake vortices. Strictly speaking, however, the Josephson coupling in these crystals is not negligible compared to the magnetic coupling because λ_c is not much larger than Λ .¹ The presence of Josephson coupling will lead to some distortion of the field profiles and to additional interaction energy, though a fully formed Josephson vortex will not exist along the kink since the kink length ρ is typically less than λ_c . Despite non-negligible Josephson coupling, the concept of pancake vortices is still qualitatively valid here and, as we have shown in Sec. IV, gives a good quantitative approximation of the field profiles measured with the Hall probe.

Pinning is essential to explain our observations. We know that there are pinning sites in the YBCO crystals for all doping values, as is typical of type II super-

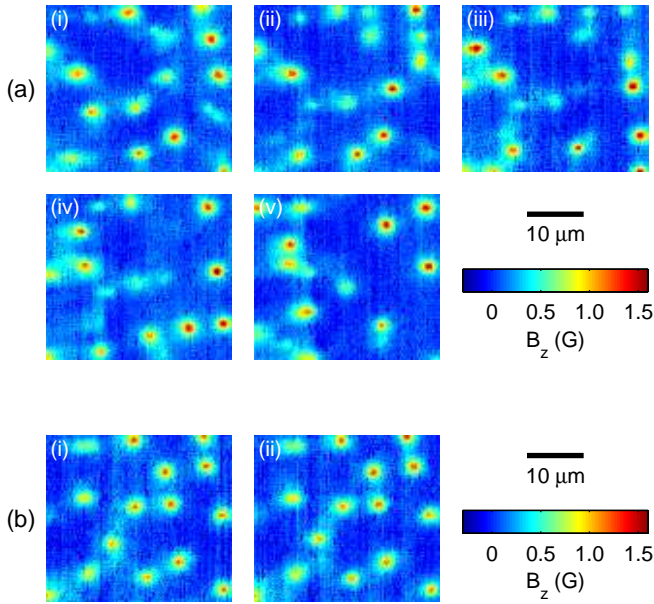


FIG. 7: (Color). Comparison of vortex movement after elevating the temperature for the $\text{YBa}_2\text{Cu}_3\text{O}_{6.375}$ crystal cooled in tilted and perpendicular fields. $T_c = 14.4$ K. (a) Field-cooled in $H_x = 2.0$ Oe and $H_z = 0.25$ Oe to $T = 3$ K. Image (i) was taken after the field was turned off. After thermal cycling sequentially to (ii) 6.6 K, (iii) 8.0 K, (iv) 9.8 K, and (v) 12.2 K. (b) The sample was field-cooled in $H_x = 0$ and $H_z = 0.25$ Oe to $T = 3$ K. Image (i) was taken after the field was turned off. (ii) After thermal cycling to 11.8 K. $T = 3.0$ K for all images.

conductors, because vortices remain in the sample after the field is turned off below T_c . In the absence of a field component in the ab -plane, magnetic coupling of the pancake vortices and any interlayer Josephson coupling favors alignment of the pancakes along the c -axis. That we observe kinked pancake stacks in the highly underdoped YBCO even after the applied field is turned off indicates that pinning of the pancakes dominates the pancake vortex arrangement. It should be noted that the calculations in Sec. IV are for kinks in otherwise straight pancake vortex stacks, but pinning may cause fluctuations in the pancake positions within a stack, distorting the field profiles.²²

To roughly quantify the strength of pinning required, we calculate the restoring force on the kinked structure. From Ref. 4, the energy required to deform a straight stack to a singly-kinked structure (in the limit of zero Josephson coupling and small layer spacing s) is

$$E_{\text{kink}}(\rho) = \left(\frac{\Phi_0}{2\pi}\right)^2 \frac{1}{4\lambda_{ab}} [(e^{-\rho/\lambda_{ab}} - 1) + \ln(\rho/\lambda_{ab}) - E_i(-\rho/\lambda_{ab}) + C], \quad (3)$$

where E_i is the exponential-integral function and C is Euler's constant. The restoring force on the kinked struc-

ture with kink length ρ found from $-dE_{\text{kink}}/d\rho$ is

$$F_{\text{kink}}(\rho) = -\left(\frac{\Phi_0}{4\pi\lambda_{ab}}\right)^2 \left[\frac{\lambda_{ab}}{\rho} - e^{-\rho/\lambda_{ab}} \left(1 + \frac{\lambda_{ab}}{\rho}\right) \right]. \quad (4)$$

For a kinked stack like that in Fig. 4 with model parameters $\rho = 5.3 \mu\text{m}$ and $\lambda_{ab} = 0.65 \mu\text{m}$, this restoring force is 80 fN. This result is for a kink deep in a crystal.

We can also consider the additional cost of a kinked stack due to finite Josephson coupling. In the limit $\gamma s < \rho < \lambda_c$, which is the case for all the kinked stacks we observed, Ref. 15 gives the energy cost of a long Josephson string connecting the two partial stacks to be of the order $E_J \approx (\Phi_0/4\pi)^2 \rho(\lambda_{ab}\lambda_c)^{-1}$. The corresponding restoring force is of the order $F_J \approx -(\Phi_0/4\pi)^2 (\lambda_{ab}\lambda_c)^{-1}$. The λ_c and λ_{ab} values obtained from Refs. 17 and 18 give this force to be approximately 3 fN for $T_c = 6$ K and 14 fN for $T_c = 15$ K. Comparing this to F_{kink} above, the added restoring force due to the Josephson string is somewhat smaller than that of the magnetic coupling. For a longer Josephson string, the energy cost of the string increases linearly with the length and the restoring force F_J remains constant. Thus, when the pinning force is large enough to compensate the restoring forces, there would be no theoretical limit to the maximum length of a metastable configuration. As a point of comparison with regards to pinning, measurements on a similar YBCO crystal with $T_c = 11$ K have estimated the required force to unpin a full vortex to be ~ 0.5 pN.²³

The calculated restoring forces would be much larger for a kinked stack in optimally doped YBCO. Using the values of $\lambda_{ab} = 0.16 \mu\text{m}$ (Ref. 24) and $\gamma = 5.5$ (Ref. 16) for near-optimally doped YBCO, F_{kink} has a maximum magnitude of 3 pN when $\rho = 2\lambda_{ab}$, or if $\rho/\lambda_{ab} = 8.2$ as it was for the highly underdoped calculations above, F_{kink} would be 1 pN. In the limit of a long Josephson string, the Josephson coupling gives an additional restoring force of magnitude $F_J = 2$ pN. These forces are much larger than for our highly underdoped YBCO, which is not surprising since optimally doped YBCO has much smaller anisotropy and much smaller λ_c , thus we expect the vortex behavior at higher doping to be less two-dimensional. Indeed, we have never seen partial vortices in Ortho-II ($T_c \approx 60$ K) or near-optimally doped YBCO crystals. Most of our measurements on these higher T_c samples were after cooling in a perpendicular field.

Pinning in these highly underdoped crystals must be strong enough to overcome the restoring force on the kinked pancake vortex stack. The origin of the pinning sites cannot be determined from our Hall probe images. They could be regions of oxygen inhomogeneity, twinning boundaries, lattice imperfections, or something else. Future studies of the pinning landscape in these crystals and in other cuprates is desirable. It is also not known how many of the pancake vortices must be pinned to support the kinked structure in the absence of an applied parallel field. However, the total force due to pinning must be of order 80 fN to compensate for the restoring force F_{kink} .

The data show that the pinning becomes less sufficient for kinked vortex formation for the later anneal stages (higher T_c). As T_c increases during the room temperature annealing, λ_{ab} decreases and so the restoring force increases. Also as the crystal anneals the oxygen chain fragments get longer, and this may have an effect on the pinning. However, since the crystals have Ortho-II ordering, there will still be many oxygen vacancies even when fully annealed. The number, spatial extent, and spatial distribution of vacancy clusters may all be changing at once during an anneal. An open question is whether oxygen inhomogeneities are necessary to see partial vortices in these samples.

The behavior of the vortices when cooled in a magnetic field with a parallel component (Figs. 6 and 7) also bears discussion. In a perpendicular field in the absence of pinning, a vortex should align parallel to the c -axis. When the field is tilted from the perpendicular, the ground state for a vortex depends on the parameters of the sample (see for example Ref. 25 for vortex lattices). In our YBCO sample $\gamma s < \lambda_{ab}$ and theory predicts a transition from a tilted to a parallel vortex lattice as the field approaches the ab -plane.²⁶ However, Benkraouda and Clem showed that beyond small angles a kinked structure can be energetically preferable to an isolated tilted vortex, which itself is unstable beyond a tilt of 52° .⁴ When our sample was cooled through T_c in a tilted field we saw many more partial vortices, which we have suggested are kinked pancake vortex stacks. Since we did not see any changes in our images when the field was turned off at low temperature, pinning must have been sufficient to sustain the pancake vortex arrangement. However, when the sample was cycled to higher temperatures (still below T_c) the flux arrangement changed as shown in Fig. 7(a). We hypothesize that at the higher temperatures the pancake vortices moved in an attempt to align along the c -axis, but in some cases became pinned again as kinked stacks upon cooling. In contrast, when the sample was cooled in a perpendicular field as in Fig. 7(b), the vortices were already pinned in their most stable state so no rearrangement occurred when cycled to higher temperature.

The fact that the partial vortices formed even when the sample was cooled in a perpendicular applied field along the c -axis (within $\sim 1^\circ$), especially for the lower T_c values, further indicates the importance of pinning. Many of the sub- Φ_0 features are elongated or show tails, which could be due to staggering of adjacent pancakes or many unresolvable kinks, indicating a complex pinning landscape. Recent improvements in the growth and preparation of these highly underdoped YBCO crystals have resulted in better homogeneity and thus perhaps less pinning compared to the earlier generation samples studied here. An ideal sample to study would be a $\text{YBa}_2\text{Cu}_3\text{O}_{6.333}$ crystal with Ortho-III inverse ordering (every third chain full). Such a highly underdoped crystal would have very few chain vacancies. Future work imaging flux in the next generation samples is desirable.

A few other researchers have reported observations of

kinked pancake vortex stacks. Grigorenko et al.² reported a Hall probe image of one “split” pancake vortex stack in a $\text{Bi}_2\text{Sr}_2\text{CaCu}_2\text{O}_{8+\delta}$ (BSCCO) crystal with $T_c = 90$ K. The kinked stack in that case was formed under a rapid change in magnetic field. Extensive vortex imaging has been done on BSCCO^{2,27,28} and typically kinked stacks such as ours have not been seen, instead combined or crossing lattices^{26,29} of pancake vortex stacks and interlayer Josephson vortices are observed. Unlike in BSCCO, we would not expect a crossing lattice to appear as the applied field approaches the ab -plane in our highly underdoped YBCO crystals because the Josephson length γs is smaller than λ_{ab} .²⁶

Beleggia et al.³ observed dumbbell-like features consistent with kinked vortices in transmission electron microscopy images of 300–400 nm thick films of optimally doped YBCO when the applied field was within 7° of parallel to the film. Our work suggests that kinked vortices may form more readily at low doping and can form even in the absence of an applied parallel field. The partial vortices we observed after cooling in only a perpendicular field could not have formed if sufficient pinning was not present. However, it is not known if pinning is always required to form kinked stacks when a sample is in a continuously applied tilted field.

In conclusion, we have observed sub- Φ_0 flux features in highly underdoped crystals of $\text{YBa}_2\text{Cu}_3\text{O}_{6+x}$ with T_c ranging from 5 to 15 K. These “partial vortices” are well described as segments of kinked stacks of 2D pancake vortices. The partial vortices were more mobile than un-kinked full vortices, formed more readily when cooled in a magnetic field with a horizontal component, and were seen most frequently for very low T_c . Our observations provide a view of vortex behavior in the highly underdoped region of the YBCO phase diagram, showing that 2D vortex behavior and an appropriate pinning landscape can produce complex flux features at the crystal surface that are distinct from conventional vortices.

Acknowledgments

We thank J.R. Clem, J.R. Kirtley, S.A. Kivelson, and V.G. Kogan for helpful discussions. Work at Stanford was funded by NSF Award No. 9875193 and the DoE contract DE-AC02-76SF00515. Work at UBC was funded by the CIAR and NSERC.

APPENDIX: PENETRATION DEPTH

We also used Hall probe images of vortices in the variable T_c $\text{YBa}_2\text{Cu}_3\text{O}_{6.375}$ crystal to estimate the in-plane penetration depth λ_{ab} , which relates to the superfluid density $n_s \propto \lambda_{ab}^{-2}$, as a function of T_c and T . Our estimates deviate from the well established linearity between T_c and $n_s(0)$ first suggested by Uemura *et al.*^{30,31} for higher doped cuprates. Our results supplement λ_{ab}

values obtained from H_{c1} measurements in Ref. 18. The unknown height of the Hall probe above the sample gives large error bars on our λ_{ab} results, and certain caveats discussed below lead us to conservatively interpret our results as upper bounds on λ_{ab} .

We chose a total of 40 different vortices in the $\text{YBa}_2\text{Cu}_3\text{O}_{6.375}$ sample for fitting, all of which appeared to be well-isolated full vortices. Each vortex was fit with the anisotropic London model in the thick crystal limit with the ab -plane parallel to the surface:^{32,33,34,35}

$$B_z(r, z) = \frac{\Phi_0}{2\pi\lambda_{ab}^2} \int_0^\infty dq \frac{q e^{-qz} J_0(qr)}{Q(Q+q)}, \quad (\text{A.1})$$

where $Q = \sqrt{q^2 + \lambda_{ab}^{-2}}$, r is the radial distance from the vortex axis, and z is the height above the sample surface. We integrated Eq. (A.1) at constant z over a $0.5 \mu\text{m}$ diameter circular area representing the Hall probe. The results are insensitive to the exact probe size and shape. We fit the vortex images using non-linear regression to extract λ_{ab} with fixed z . Free parameters were the location of the vortex center, a constant offset in the magnetic field (due to the Hall probe), and λ_{ab} . The lengths z and λ_{ab} are strongly correlated and could not both be free parameters.

In the scanning microscope $z = z_0 + \Delta z$, where z_0 is the sample-probe distance when touching, and Δz is controllable and for these measurements ranged from 0– $0.16 \mu\text{m}$. Geometric constraints give a lower bound of $z_0 \geq 0.4 \mu\text{m}$. A very conservative upper bound of $z_0 \leq 1.45 \mu\text{m}$ was obtained for this data set by fitting vortices at maximum T_c with $\lambda_{ab} = 0$ and z as a free parameter. A smaller upper bound of $z_0 \leq 1.3 \mu\text{m}$ was obtained by assuming $\lambda_{ab}(0)$ is at least as large as in optimally doped YBCO.²⁴ All vortices were fit with a range of z_0 values. Fit results are reported here with the typical value $z_0 = 0.8 \mu\text{m}$, with systematic error bars determined by fits with $z_0 = 0.4 \mu\text{m}$ and $z_0 = 1.3 \mu\text{m}$.

For four vortices we also took Hall probe images while warming to investigate temperature dependence. The inset of Fig. 8 shows $\lambda_{ab}(T)$ at the minimum and maximum T_c stages. Within our systematic and statistical errors, it is not possible to extract the details of $\lambda_{ab}(T)$ at low temperatures. The penetration depth appears approximately constant for temperatures below $T_c/2$. Thus we approximate $\lambda_{ab}(0)$ by $\lambda_{ab}(T_{\min})$ with $T_{\min} \sim 2 \text{ K}$ for $T_c < 12 \text{ K}$ and $T_{\min} \sim 4 \text{ K}$ for higher T_c .

Our $\lambda_{ab}(T_{\min})$ versus T_c results are shown in Fig. 8. The dominant sources of error are the uncertainty in z_0 (which will be the same for all data points) and the calibration of the probe's Hall coefficient, $R_H = 0.115 \pm 0.015 \Omega/\text{G}$ (which may fluctuate from cooldown to cooldown). Fits with the z_0 extremes show that the corresponding λ_{ab} error, indicated by the double arrow in the upper left of Fig. 8, is roughly constant for all data points. The uncertainty in R_H translates to a λ_{ab} error of roughly $\pm 8\%$ of $z + \lambda_{ab}$. The in-plane penetration depth decreased as T_c increased. For example, at $T_c = 6.5 \text{ K}$,

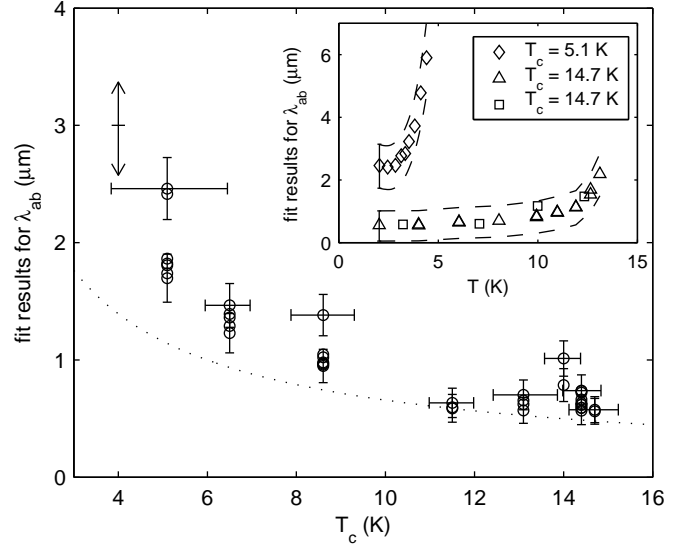


FIG. 8: Fit results for low-temperature λ_{ab} versus T_c for the $\text{YBa}_2\text{Cu}_3\text{O}_{6.375}$ crystal, obtained from fits to scanning Hall probe images of 40 different vortices at eight T_c stages of a room temperature annealing. The fitted λ_{ab} is an upper bound on the true $\lambda_{ab}(0)$. Horizontal bars indicate the resolution-limited full width of the superconducting transition for each T_c . Vertical error bars (shown only for the extreme data points) are from uncertainty in the probe calibration. A systematic error from uncertainty in the minimum sample-probe distance z_0 could shift the full data set by the extent indicated by the double arrow at $T_c = 4 \text{ K}$. Data points shown are with $z_0 = 0.8 \mu\text{m}$. For comparison, the dotted curve is from the fit to $H_{c1}(T_c)$ from Ref. 18 as discussed in the text. Inset: Temperature dependence of the λ_{ab} results for two T_c values. For each data set shown, λ_{ab} was obtained from fits to scanning Hall probe images of an individual vortex as T increased. The vortices disappeared before T_c . The dashed lines indicate the maximum extent the data sets could be shifted due to systematic errors.

the average value is $\lambda_{ab} = 1.35 \pm 0.18^{+0.37}_{-0.43} \mu\text{m}$, while for the highest $T_c = 14.7 \text{ K}$ it is $\lambda_{ab} = 0.57 \pm 0.11^{+0.34}_{-0.40} \mu\text{m}$, where the quoted errors are from the uncertainties in R_H and z_0 , respectively.

The in-plane penetration depth λ_{ab} is actually a combination of λ_a and λ_b , which are not equal in YBCO. The λ_a/λ_b anisotropy has been measured to be slightly larger than unity in higher doped samples (see for example Ref. 36). In-plane anisotropy would lead to a distortion of the otherwise circular field profile of a vortex aligned along the c -axis. In principle, our approach could be used to obtain separate values for λ_a and λ_b if it was performed on a detwinned crystal.

There are several caveats to our λ_{ab} measurements. First, it is possible that some of the full vortices identified for fitting were actually partial vortices, especially at the lowest T_c values where fewer full vortices were available for comparison. If a partial vortex stack was fit with Eq. (A.1), the resulting λ_{ab} value would be falsely high.

At higher T_c , many more full vortices of consistent appearance were observed. However, it cannot be ruled out that the pancake vortices in the “straight” stacks were not completely axial but rather pinned in a staggered manner resulting in a more spread out vortex field profile. If this were the case, our fits would yield falsely high λ_{ab} values since Eq. (A.1) is for a straight vortex. Thus the most conservative approach to our fit results is to take the values shown in Fig. 8 as *upper bounds* on the true values of λ_{ab} .

For $T_c > 10$ K, our $\lambda_{ab}(T_{\min})$ values obtained from vortex fits are close to the values calculated from the low T_c fit $H_{c1}(0) = 0.366 T_c^{1.64}$ (Oe) from Ref. 18, as shown by the dotted curve in Fig. 8. For $T_c < 10$ K, our values lie slightly above the curve. However, as discussed

above, our values should conservatively be treated as upper bounds, so there is not a discrepancy with Ref. 18.

Our λ_{ab} estimates, along with the results of Ref. 18, give a larger T_c for a given superfluid density in the highly underdoped regime than predicted by the Uemura relation $T_c \propto n_s(0)$. Other recent experiments have also shown deviations from this relation, such as Pereg-Barnea *et al.*³⁶ in higher doped YBCO crystals and Zuez *et al.*³⁷ in underdoped YBCO films. These data indicate that thermal phase fluctuations alone cannot explain the suppressed superfluid density in underdoped cuprates. Herbut and Case³⁸ proposed that low temperature nodal quasiparticles and vortex fluctuations near T_c can explain the observed nonlinearity between T_c and $n_s(0)$.

-
- * Address as of March 2008: Department of Physics & Astronomy, Johns Hopkins University, Baltimore, MD 21218
† Electronic address: kmoler@stanford.edu
- ¹ J. R. Clem, Phys. Rev. B **43**, 7837 (1991).
 - ² A. N. Grigorenko, S. J. Bending, A. E. Koshelev, J. R. Clem, T. Tamegai, and S. Ooi, Phys. Rev. Lett. **89**, 217003 (2002).
 - ³ M. Beleggia, G. Pozzi, A. Tonomura, H. Kasai, T. Matsuda, K. Harada, T. Akashi, T. Masui, and S. Tajima, Phys. Rev. B **70**, 184518 (2004).
 - ⁴ M. Benkraouda and J. R. Clem, Phys. Rev. B **53**, 438 (1996).
 - ⁵ A. K. Geim, S. V. Dubonos, I. V. Grigorieva, K. S. Novoselov, F. M. Peeters, and V. A. Schweigert, Nature (London) **407**, 55 (2000).
 - ⁶ J. R. Kirtley, P. Chaudhari, M. B. Ketchen, N. Khare, S.-Y. Lin, and T. Shaw, Phys. Rev. B **51**, 12057 (1995).
 - ⁷ J. Mannhart, H. Hilgenkamp, B. Mayer, C. Gerber, J. R. Kirtley, K. A. Moler, and M. Sigrist, Phys. Rev. Lett. **77**, 2782 (1996).
 - ⁸ R. Liang, D. A. Bonn, and W. N. Hardy, Physica (Amsterdam) **304C**, 105 (1998).
 - ⁹ R. Liang, D. A. Bonn, W. N. Hardy, J. C. Wynn, K. A. Moler, L. Lu, S. Larochelle, L. Zhou, M. Greven, L. Lurio, et al., Physica (Amsterdam) **383C**, 1 (2002).
 - ¹⁰ R. Liang, private communication.
 - ¹¹ J. W. Guikema, Ph.D. Thesis, Stanford University (2004).
 - ¹² A. M. Chang, H. D. Hallen, L. Harriott, H. F. Hess, H. L. Kao, J. Kwo, R. E. Miller, R. Wolfe, J. van der Ziel, and T. Y. Chang, Appl. Phys. Lett. **61**, 1974 (1992).
 - ¹³ D. Davidović, S. Kumar, D. H. Reich, J. Siegel, S. B. Field, R. C. Tiberio, R. Hey, and K. Ploog, Phys. Rev. Lett. **76**, 815 (1996).
 - ¹⁴ A. Oral, S. J. Bending, and M. Henini, J. Vac. Sci. Technol. B **14**, 1202 (1996).
 - ¹⁵ J. R. Clem, J. Supercond. **17**, 613 (2004).
 - ¹⁶ G. J. Dolan, F. Holtzberg, C. Feild, and T. R. Dinger, Phys. Rev. Lett. **62**, 2184 (1989).
 - ¹⁷ A. Hosseini, D. M. Broun, D. E. Sheehy, T. P. Davis, M. Franz, W. N. Hardy, R. Liang, and D. A. Bonn, Phys. Rev. Lett. **93**, 107003 (2004).
 - ¹⁸ R. Liang, D. A. Bonn, W. N. Hardy, and D. Broun, Phys. Rev. Lett. **94**, 117001 (2005).
 - ¹⁹ K. E. Gray, D. H. Kim, B. W. Veal, G. T. Seidler, T. F. Rosenbaum, and D. E. Farrell, Phys. Rev. B **45**, 10071 (1992).
 - ²⁰ J. R. Clem, Physica (Amsterdam) **235–240C**, 2607 (1994).
 - ²¹ R. G. Mints, V. G. Kogan, and J. R. Clem, Phys. Rev. B **61**, 1623 (2000).
 - ²² A. N. Grigorenko, S. J. Bending, G. D. Howells, and R. G. Humphreys, Phys. Rev. B **62**, 721 (2000).
 - ²³ B. W. Gardner, J. C. Wynn, D. A. Bonn, R. Liang, W. N. Hardy, J. R. Kirtley, V. G. Kogan, and K. A. Moler, Appl. Phys. Lett. **80**, 1010 (2002).
 - ²⁴ D. N. Basov, R. Liang, D. A. Bonn, W. N. Hardy, B. Dabrowski, M. Quijada, D. B. Tanner, J. P. Rice, D. M. Ginsberg, and T. Timusk, Phys. Rev. Lett. **74**, 598 (1995).
 - ²⁵ A. E. Koshelev, Phys. Rev. B **71**, 174507 (2005).
 - ²⁶ L. N. Bulaevskii, M. Ledvij, and V. G. Kogan, Phys. Rev. B **46**, 366 (1992).
 - ²⁷ A. Grigorenko, S. Bending, T. Tamegai, S. Ooi, and M. Henini, Nature (London) **414**, 728 (2001).
 - ²⁸ S. J. Bending and M. J. W. Dodgson, J. Phys.: Condens. Matter **17**, R955 (2005).
 - ²⁹ A. E. Koshelev, Phys. Rev. Lett. **83**, 187 (1999).
 - ³⁰ Y. J. Uemura, G. M. Luke, B. J. Sternlieb, J. H. Brewer, J. F. Carolan, W. N. Hardy, R. Kadono, J. R. Kempton, R. F. Kiefl, S. R. Kreitzman, et al., Phys. Rev. Lett. **62**, 2317 (1989).
 - ³¹ Y. J. Uemura, L. P. Le, G. M. Luke, B. J. Sternlieb, W. D. Wu, J. H. Brewer, T. M. Riseman, C. L. Seaman, M. B. Maple, M. Ishikawa, et al., Phys. Rev. Lett. **66**, 2665 (1991).
 - ³² J. Pearl, J. Appl. Phys. **37**, 4139 (1966).
 - ³³ V. G. Kogan, A. Y. Simonov, and M. Ledvij, Phys. Rev. B **48**, 392 (1993).
 - ³⁴ J. R. Kirtley, V. G. Kogan, J. R. Clem, and K. A. Moler, Phys. Rev. B **59**, 4343 (1999).
 - ³⁵ J. R. Kirtley, C. C. Tsuei, K. A. Moler, V. G. Kogan, J. R. Clem, and A. J. Turberfield, Appl. Phys. Lett. **74**, 4011 (1999).
 - ³⁶ T. Pereg-Barnea, P. J. Turner, R. Harris, G. K. Mullins, J. S. Bobowski, M. Raudsepp, R. Liang, D. A. Bonn, and W. N. Hardy, Phys. Rev. B **69**, 184513 (2004).
 - ³⁷ Y. Zuev, M. S. Kim, and T. R. Lemberger, Phys. Rev.

Lett. **95**, 137002 (2005).

- ³⁸ I. F. Herbut and M. J. Case, Phys. Rev. B **70**, 094516 (2004).